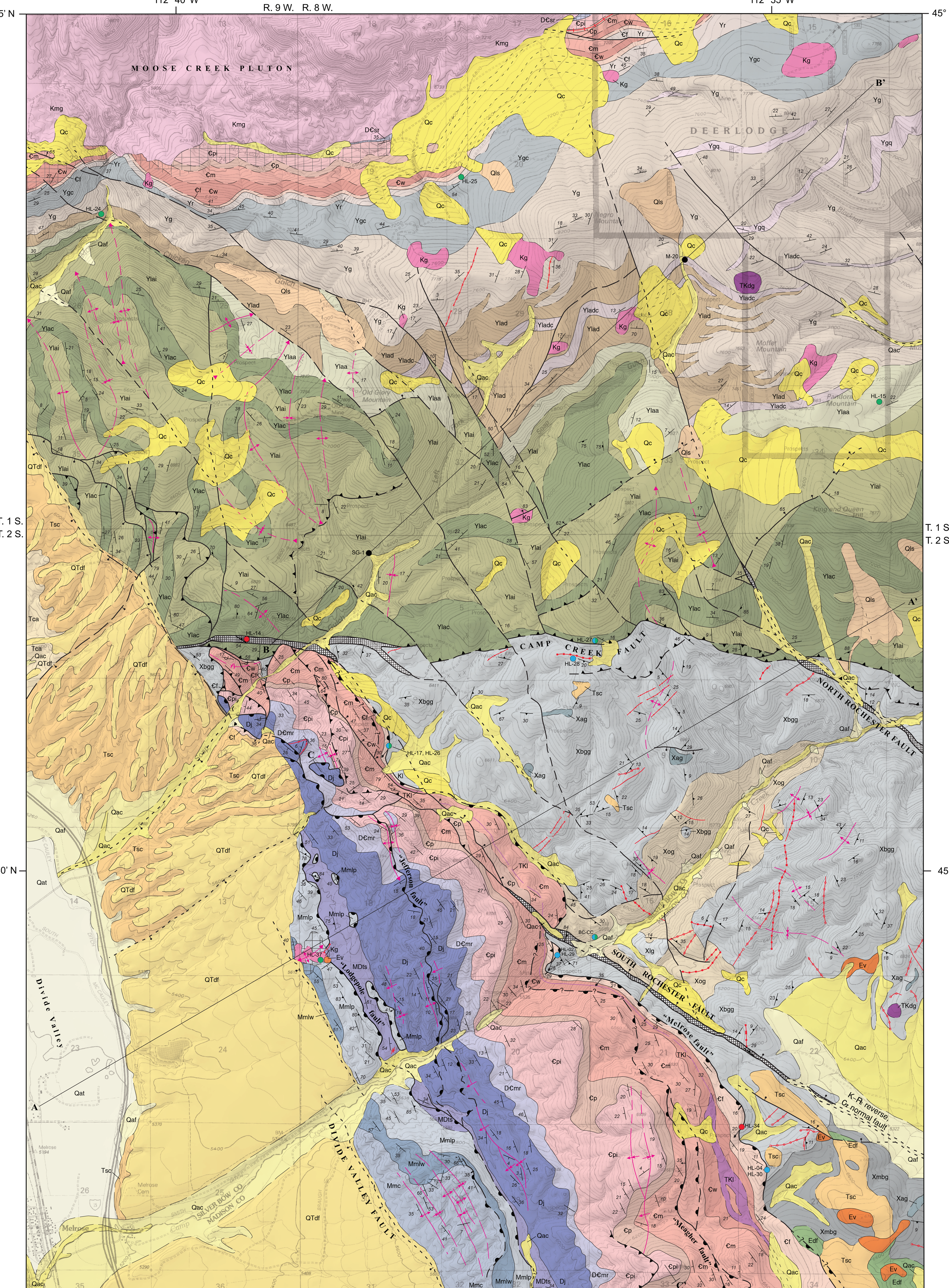

SCALE 1:24 000

CONTOUR INTERVAL 40 FEET
DATUM IS MEAN SEA LEVEL

Base maps produced by the United States Forest Service and United States Geological Survey Melrose and Wickiup Creek 1:24,000 scale quadrangle maps
Control by: USGS, NOS/NOAA and USFS
Compiled from aerial photographs taken 1956 and 1995
Field checked: 1961
Projection: Polyconic
Grid: 1000 meter Universal Transerve Mercator Zone 12
UTM grid declination: 1° 40′ West
1961 Magnetic North Declination: 18.87° East
2022 Magnetic North Declination: 12.15° East
Vertical Datum: National Geodetic Vertical Datum of 1929
Horizontal Datum: 1983 North American Datum
Shaded relief created from 3 meter digital elevation model from U.S. Geological Survey National Elevation Dataset

Research supported by the U.S. Geological Survey EDMAP Program, under EDMAP award number G20AC00227.
GIS production and map layout: Chance B. Ronemus, Montana State University
This map sheet underwent MBMG review by Colleen Elliott and Katie McDonald

Previous Mapping Sources
1. Richard and Pardee (1926)
2. Brumbaugh (1973)
3. Brandon (1984)
4. Ruppel and others (1983)
5. Smedes and others (1988)
6. O'Neill and others (1996)
7. Vuke (2004)
8. Elliott and McDonald (2009)
9. McDonald and others (2012)

Location Map and Previous Mapping

Dewy	Tucker Creek	Mount Humbug 4, 7 = 1, 3	Pipestone Pass
Cattle Gulch	1, 2, 3, 4, 5, 6, 7, 8 9, 10 Melrose	2, 4, 5, 6 7, 8, 9, 10 Wickiup Creek	Table Mountain
Storm Peak	Earls Gulch	Nez Perce Hollow	Twin Bridges SW

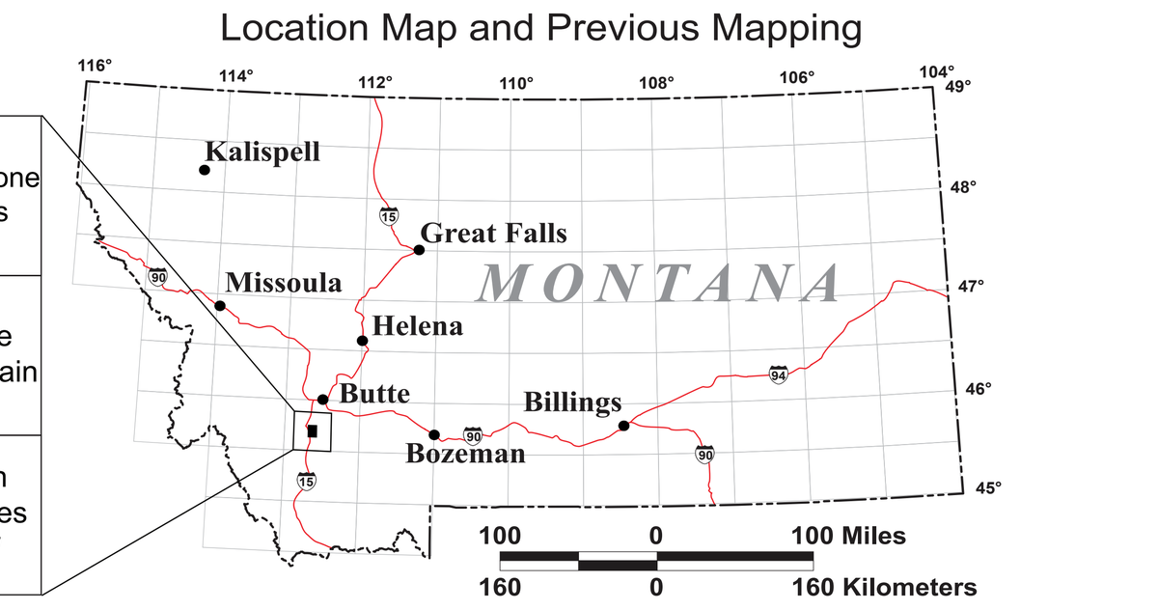

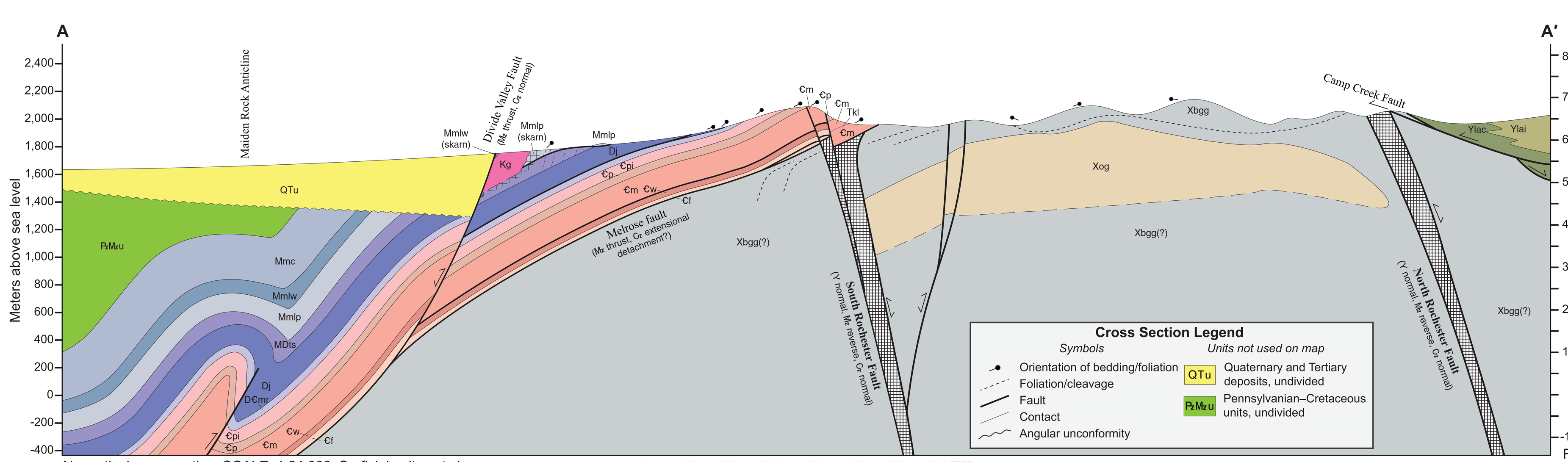

No vertical exaggeration. SCALE: 1:24,000. Surficial units not shown.

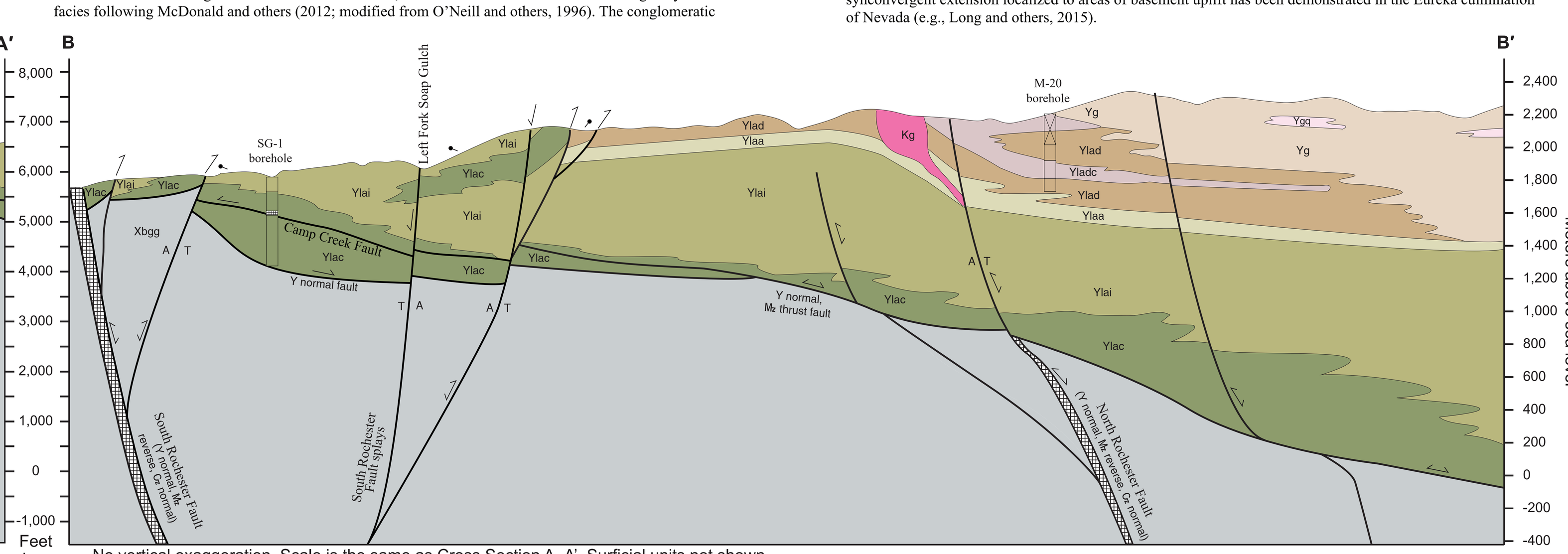

No vertical exaggeration. Scale is the same as Cross Section A–A′. Surficial units not shown.

CORRELATION DIAGRAM

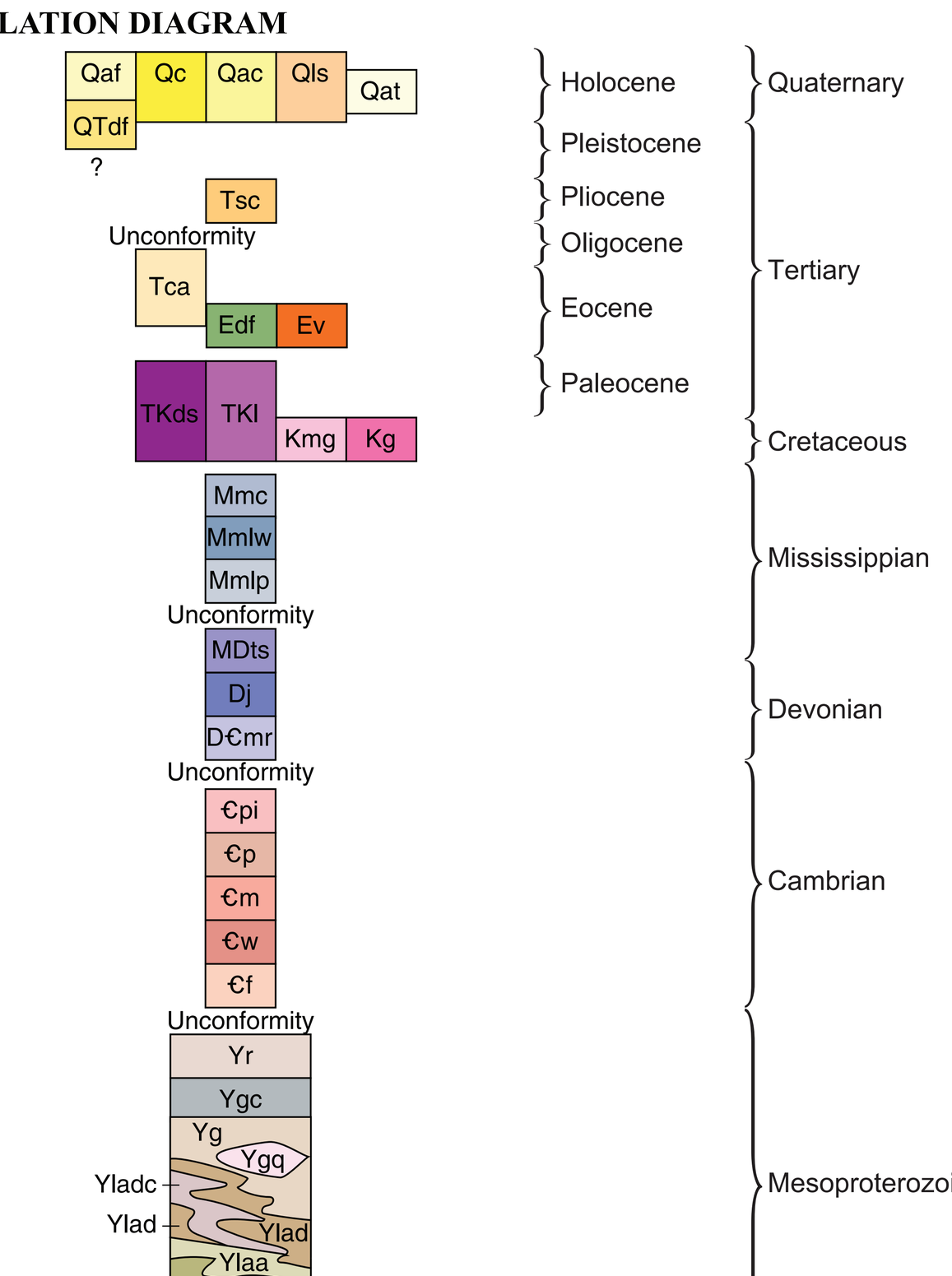

MAP SYMBOLS

- High-angle fault, kinematics uncertain; all linear features are shown by long dash where approximately located; short dash where inferred; dotted where concealed
- Thrust fault; teeth on upthrown block
- Bedding sub-parallel fault; kinematics uncertain; potentially reactivated (see structural summary); semi-circles on hanging wall
- Normal fault; ball and bar on downthrown side
- Shear zone
- Contact
- Anticline; showing trace of axial plane and plunge direction, where known
- Syncline; showing trace of axial plane and plunge direction, where known
- Monocline; showing trace of axial plane
- Anticlinal bend on monocline; showing trace of axial plane
- Extent of contact metamorphism associated with intrusives
- Quartz Vein
- Felsic dike
- Basalt-andesite dike
- Diabase dike (Mesoproterozoic)
- Pegmatite dike in basement rock
- Mafic dike in basement rock
- Lamprophyric sill (TKl)
- Strike and dip of inclined bedding, all measurements averaged when closely spaced
- Strike and dip of overturned bedding
- Strike and dip gneissic banding in metamorphic rocks; slately or fracture cleavage in sedimentary rock
- Strike and dip of fracture or jointing
- Trend and plunge of slickenline on fault surface
- Strike and dip of fault surface
- HL-15 Zircon U-Pb sample
- HL-29 Thermochronology sample
- HL-34 Thin section sample
- SG-1 Logged exploration borehole

INTRODUCTION

The Highland Mountains, located ~20 km south of Butte, Montana, comprise a representative microcosm of the geology of southwestern Montana, situated in a zone of overlap between tectonic provinces including the Paleoproterozoic Big Sky orogen, Mesoproterozoic Belt Basin, and Sevier, Laramide, and later extensional components of the Phanerozoic North American Cordillera (e.g., DeCelles, 2004; Kulik and Schmidt, 1988; Lageson, 1989; O'Neill and others, 1990). This billion-year history of polyphase deformation has superposed structures of various ages and styles, resulting in complex structural geometries and relationships which remain relatively poorly constrained. This project involved targeted 1:24,000 scale geologic mapping of two contiguous half 7.5′ quadrangles in the western Highland Mountains: the eastern half of the Melrose 7.5′ quadrangle and the western half of the Wickiup Creek 7.5′ quadrangle. This mapping revisits areas of complexity identified during STATEMAP 1:100,000 scale mapping by the Montana Bureau of Mines and Geology (MBMG) of the encompassing Butte South 30′ x 60′ quadrangle (McDonald and others, 2012). Detailed mapping was paired with geo/thermochronology (Figures 1–2), logging of exploration boreholes (Figure 3), and (micro)structural analysis (Figures 4–7) to address these complexities and better constrain the structural evolution of the study area.

PREVIOUS MAPPING

The Melrose and Wickiup Creek 7.5' quadrangles are included in the previously mapped Dillon 1° x 2° quadrangle (Ruppel and others, 1983, 1:250,000 scale) and the Butte South 30' x 60' quadrangle (McDonald and others, 2012, 1:100,000 scale). The central and southern Highland Mountains were mapped by the USGS (O'Neill and others, 1996, 1:50,000 scale). Mapping of portions of the study area north of Camp Creek was included in an MBMG geologic map and geohazards assessment of Silver Bow county (Elliott and McDonald, 2009, 1:50,000 scale), a USGS map with focus on the Boulder Batholith (Smedes and others, 1988, 1:200,000 scale), and an MBMG map focused on Tertiary units in the Divide area (Vuke, 2004, 1:50,000 scale). Early USGS mapping assessing economic phosphorous potential included the western portion of the study area (Richards and Pardee, 1926, 1:62,500 scale). Portions of the study area were included in Ph.D. dissertations involving detailed mapping of the Moose Creek pluton (Andretta, 1961, 1:20,000 scale) and the McCartney thrust salient (Brandon, 1984; Brumbaugh, 1973, both 1:24,000 scale).

ANALYTICAL METHODS (Geochronology and Thermochronology)

Zircon U-Pb geochronology was conducted on four samples of Belt Supergroup rock (HL-15, HL-24, HL-25, HL-27) to constrain sedimentary provenance (Figure 1A), a sample of metamorphic basement rock (HL-26) to constrain the age of local basement (Figure 1A), and a sample from a pluton cross-cutting a fault in the western study area (HL-37) to constrain the minimum timing of slip on this fault (Figure 1B). U-Pb geochronology was conducted by laser ablation inductively coupled plasma mass spectrometry at the Arizona LaserChron Center, University of Airzona.

Apatite and zircon [U-Th(-Sm)]/He thermochronology was conducted to assess the thermal history of the Highland Mountains. Paired samples were collected from the Cambrian Flathead Sandstone (HL-02, HL-04, and HL-17) and proximal underlying basement rock (HL-26, HL-29, and HL-30) (Figure 2A) and from the proximal footwall (HL-28) and hanging-wall (HL-27) of the Camp Creek fault (Figure 2B). [U-Th(-Sm)]/He dating of zircon and apatite grains was conducted at the University of Illinois Urbana-Champaign Helium Analysis Laboratory and the University of Colorado (U-Th)/He Thermochronology Laboratory, respectively. Thermochronology data were modeled using QTQt (Gallagher, 2012). The full U-Pb, AHe and ZHe datasets and a detailed description of analytical methods are available in the MBMG Geoarchive database.

MAP UNITS

Rocks in the study area consist mainly of Paleoproterozoic metamorphic basement rocks, Mesoproterozoic, Paleozoic, and Tertiary sedimentary rocks, and Cretaceous igneous rocks. The map units and their age relationships are described in the Descriptions of Map Units and Correlation Diagram sections of this plate. Our interpretations of the Phanerozoic stratigraphy do not differ significantly from recent previous work in the study area (e.g., Hanson, 1952; McDonald and others, 2012; O'Neill and others, 1996; Vuke, 2004). New constraints on Precambrian rocks are described below.

Metamorphic Rocks

Biotite-garnet gneiss comprises the volumetrically dominant basement lithology in the study area. Zircon U-Pb geochronology results yielded a maximum depositional age (MDA) of 1794.2 ± 3.0 Ma (Figure 1A; sample HL-26), indicating Paleoproterozoic deposition of the unit's sedimentary protolith. The biotite-garnet gneiss is intruded by a large (ca. 5 km²) sill-like orthogneiss body near Camp Creek. This unit yielded a zircon U-Pb weighted mean age of 1797.7 ± 16.5 Ma (Carrapa and others, 2019). This age overlaps at uncertainty with that of HL-26, suggesting intrusion soon after deposition of the biotite-garnet gneiss protolith. New ages for these units are coeval with the the Big Sky Orogeny (Condit and others, 2015) and may reflect associated synorogenic deposition and magmatism.

Mesoproterozoic Belt Supergroup Rocks

Precambrian sedimentary rocks in the map area, which are assigned to the Mesoproterozoic Belt Supergroup, are confined to a generally north-dipping panel north of the Camp Creek fault. The lower portion of this succession is assigned to the LaHood Formation, which we have subdivided into lithologically distinct facies following McDonald and others (2012; modified from O'Neill and others, 1996). The conglomeratic facies is thickest near the Camp Creek fault and grades northward into the finer-grained intermediate siliciclastic facies and argillite and siltite facies. The latter is in turn overlain by the dark argillite and carbonate facies, likely correlative with the Newland Formation in the northern Helena Embayment (Fox, 2017; McDonald and others, 2012; Nilsen, 1991). Intertonguing relationships are observed between all stratigraphically adjacent facies. The dark argillite and carbonate facies intertongues with the overlying lower argillite member of the Greyson Formation. Lithologic and facies thickness variations occuring within these units across NW-striking faults have been interpreted as evidence of syn-depositional normal faulting (O'Neill and others, 1986). These variations are less pronounced to absent in the upper calcsilicate member of the Greyson Formation and the overlying Ravalli Group (following McDonald and others, 2012).

Detrital zircon U-Pb ages from the LaHood Formation and the Ravalli Group are dominated by an age-probability peak centered at 1785 ± 7 Ma (Figure 1A). This peak is similar in age to the main zircon U-Pb age population of the Paleoproterozoic biotite-garnet gneiss (1794.2 ± 3.0 Ma; Figure 1A) and orthogneiss (1797.7 ± 16.5 Ma; Carrapa et al., 2019), suggesting dominance of local sediment sources. Increased input from distal sources through time is suggested by an up-section increase in Archean zircon abundance (Figure 1A). Observed map patterns and provenance trends are consistent with previous interpretations of the various facies of the LaHood Formation as portions of a submarine fan/slope/shelf system deposited in compartmentalized sub-basins with local sediment supply (Fox, 2017; Nilsen, 1991). The geometry of sub-basins was likely controlled by both E-W striking normal faults (i.e., Perry line of Winston, 1986) and smaller-scale NW-striking normal faults. The basin became increasingly integrated as movement on the latter faults ceased, reflected by decreased along-strike variation in facies thicknesses and increased input of distally derived zircon up section.

Pyrite and chalcopyrite occurring in stratiform morphologies were observed within limestone and dolomitic shale intervals of the dark argillite and carbonate facies of the LaHood Formation (Figure 3A–C). Mineralization is of similar character to the Black Butte copper deposits, hosted in the likely correlative Newland Formation near White Sulfur Springs, MT. The Black Butte deposits have been previously characterized as a sediment-hosted stratiform copper deposit, with fluids supplied by syn-depositional normal faults depositing metals on the sea floor (White and others, 2014; Zieg, 1981). Sulfides in the dark argillite and carbonate facies of the LaHood Formation in the study area may have formed in a similar context.

STRUCTURAL SUMMARY

Five main fault sets were recognized in the map area: (1) the north-dipping Camp Creek Fault, carrying Belt Supergroup rocks; (2) NW-striking and steeply dipping faults involving basement rock; (3) a sheared zone at the base of the Paleozoic section; (4) SW-dipping, bedding sub-parallel faults involving Paleozoic rocks; and (5) Cenozoic normal faults bounding the western range front. This work focused on sets (1–4), described below.

1) Camp Creek Fault

The Camp Creek Fault (CCF) juxtaposes Mesoproterozoic rocks of the LaHood Formation against Proterozoic basement rock and Paleozoic sedimentary rock. The SG-1 borehole near Soap Gulch (sec. 6, T. 2 S., R. 8 W.) intersected a ~40 m zone of fault gouge and breccia at ~230–270 m depth, which we interpret to constitute the CCF. Fault rock lithologies observed in this borehole (Figure 3D) suggest at least its most recent phase of slip was dominantly brittle. A three-point problem using surface exposures and the inferred borehole intersection indicates the fault plane dips 26° towards an azimuth of 009°. Early interpretations of the CCF involved km-scale right-lateral slip (e.g., Ruppel and Lopez, 1984). NNW-trending folds and WSW-dipping thrust faults in the LaHood Formation are consistent with some degree of SSW-NNE shortening of the Belt Supergroup section. However, if set (2) faults associated with growth geometries in the Belt Supergroup correlate into the SRF and NRF as discussed below, these faults comprise piercing points precluding significant right-lateral slip on the CCF (e.g., O'Neill and others, 1986; O'Neill, 1995). Instead, predominantly south-directed thrusting of the CCF was interpreted by O'Neill (1995) based on the orientation of shears and folds within the CCF fault zone. We map overturned lower Paleozoic strata in the north limb of a fold in the proximal footwall of, and trending sub-parallel to, the CCF. We interpret this to reflect fault-propagation folding during south-directed thrusting of the CCF. Additionally, a component of left-lateral movement on the CCF was suggested by O'Neill and others (1996) and McDonald and others (2012) on the basis of apparent S-shaped curvature of set (2) faults across the CCF and shear fabrics within the CCF shear zone, respectively.

The CCF has previously been interpreted as reactivating the north-dipping Mesoproterozoic normal fault system bounding the southern margin of the Helena Embayment of the Belt Supergroup (e.g., McDonald and others, 2012; McMannis, 1963). However, the SG-1 borehole intersected ~320 m of LaHood Formation conglomeratic facies below the ~40 m fault zone described above. If this fault zone is the CCF, this suggests the fault duplicates portions of the LaHood Formation and must therefore dip more shallowly than the Mesoproterozoic fault bounding the southern margin of the basin, although the two may merge at depth (e.g., Schmidt and Garihan, 1983). Thermal history model results for sample HL-27 in the CCF hanging-wall indicates cooling mainly between ~80 Ma and 60 Ma (Figure 2B). However, the modeled thermal history for this sample is poorly constrained and overlaps with slower cooling modeled for sample HL-28 from the CCF foot-wall (Figure 2B), suggesting modeled cooling may not be directly related to slip on the CCF.

2) South Rochester Fault, North Rochester Fault, and related splays

Fault set (2) consists of the South Rochester Fault (SRF), North Rochester Fault (NRF), and related fault splays. These faults are expressed mainly as broad (~10–200 m), altered shear zones within the Paleoproterozoic basement. In the northern portion of the map area, a series of faults with similar orientation offset rocks in the hanging-wall of the CCF. The LaHood through lower Greyson formations exhibit apparent growth geometries associated with these faults, which appear to offset the CCF and trace southward into the SRF and NRF systems in Proterozoic basement (O'Neill and others, 1996).

North of Camp Creek, the SRF can be traced into the Paleozoic section, where it branches into a series of splays. One splay duplicates portions of the Pilgrim, Park, and Meagher Formations (Figure 4A). Symmetric shear fabrics with south-plunging quartz aggregate lineations within the SRF and NRF shear zones have been interpreted to record a phase of east-side-up, sinistral-oblique motion, likely producing this observed reverse displacement (McDonald and others, 2012; O'Neill, 1995). Brittle deformation was observed in a thin section from the SRF shear zone near Soap Gulch (Figure 5A). Time-temperature (t-T) model results for samples from the proximal hanging-wall of the SRF (Carrapa et al., 2019) indicate rapid cooling constrained between ~95 Ma and 75 Ma—preceding cooling of samples in the footwall (Figure 2A). This cooling likely reflects erosional exhumation of the SRF hanging-wall driven by reverse faulting. Other splays of the SRF within the Paleozoic section exhibit normal displacement (Figure 3B), and the SRF and NRF offset units as least as young as Eocene further south, indicating extensional reactivation during Cenozoic time (McDonald and others, 2012; O'Neill and others, 1996; this study). Collectively, these observations suggest set (2) faults were activated during Mesoproterozoic, late Mesozoic, and Cenozoic time with normal, reverse, and normal slip, respectively.

3) Melrose fault

The contact between the Cambrian Flathead Formation and underlying Paleoproterozoic basement rock has previously been interpreted as depositional (Hanson, 1952; O'Neill and others, 1996; Thomas, 2007). However, we document evidence of deformation along this contact. Near Camp Creek, the contact is marked by layer of vein quartz breccia (Figure 4C). Thin sections sampled from below the contact contain fractured quartz and iron oxide grains within chlorite-clay matrix (Figure 5B). Slickenlines observed on the base of the Flathead Formation define a mean lineation (n = 18) plunging toward 223° at 27 ± 7° (Figure 6A). Collectively, these observations are consistent with a component of brittle dip-slip shear. We informally refer to this shear zone as the Melrose fault, which defines a mean plane dipping 22° toward an azimuth of 226° (Figure 6A).

We also observed evidence consistent with a ductile component of deformation accomodated by this shear zone. Basement rock in the footwall grades from relatively unaltered biotite-garnet gneiss to highly deformed chlorite schist near the contact with the Flathead Formation (Figure 4C). Foliation of basement rock exhibits progressive rotation with proximity to the contact, becoming sub-parallel to the shear zone (Figure 6B). Vein-related antithetic slip-reverse drag folds and S-C fabrics observed within the shear zone are consistent with extensional, top-WSW ductile shear (Figure 4C; Druguet, 2019). Thermal history modeling results suggest rocks in the footwall of the Melrose fault footwall experienced cooling between ~75 Ma and 55 Ma, while those in the hanging-wall cooled between ~65 and 50 Ma (Figure 2A). This discrepancy in modeled cooling time may indicate tectonic exhumation of the footwall via extensional unroofing. However, the modeled timing of cooling of rocks on either side of the fault overlaps at uncertainty. North of Camp Creek, two quartzite units of the Cambrian Flathead Formation are separated by shear zones defining a mean plane (n = 5) dipping 29° toward an azimuth of 222°—a similar orientation to the main Melrose fault (Figure 6A). Apparent tectonic duplication of the quartzite units by this shear zone may indicate a compressional phase of deformation, possibly pre-dating the extensional episode discussed above. The kinematics and significance of the Melrose Fault remain not fully constrained. Interpretations are discussed in more detail in the following section.

4) Bedding sub-parallel faults within Paleozoic section

The main faults of set (4) are here informally referred to as the Meagher, Jefferson, and Lodgepole faults. These faults are generally sub-parallel to the bedding of the Paleozoic rocks they carry, exhibit relative minor (≤ 100 m) stratigraphic separation, and are associated with small damage zones (≤ 2 m). This led early workers to interpret the Paleozoic section in the study area as unfaulted (e.g., Hanson, 1952). Net stratigraphic separation across set (4) faults transitions from positive (i.e., repeated section) to negative (i.e., deleted section) along-strike (Figure 7). Constraints on the kinematics and timing of set (4) faults is summarized below.

In the southern portion of the map area, the Jefferson and Meagher faults duplicate section. The axial traces of map-scale folds within the Paleozoic section trend sub-parallel to the traces of these faults and, in places, comprise paired footwall synclines and hanging-wall anticlines consistent with compressional fault-propagation folding. In the Lodgepole fault zone, pervasive near-vertical NNW-SSE striking pressure solution cleavage of the Mississippian Lodgepole Formation (Figure 6C) is involved in a top-WNW asymmetric fold, the upright limb of which shows stacking of imbricated horses (Figure 4D). The Lodgepole fault is cut by a granodioritic pluton, yielding a weighted mean zircon U-Pb age of 74.4 ± 0.4 | 0.72 Ma (MSWD = 0.99; Figure 1B). This constrains the maximum age of slip on the Lodgepole fault to pre-Maastrichtian time, during which time shortening is widely documented in the Montana–Idaho fold-thrust belt. The above observations are consistent with compressional deformation accomodated by set (4) faults.

By contrast, younger-on-older relationships exist across the northern portions of set (4) faults in the map area. A strike-parallel stratigraphic separation diagram for the Meagher fault shows an abrupt transition from null or positive stratigraphic gap to negative stratigraphic gap northward across the fault's intersection with the trace of the SRF (Figures 4B and 7). Stratigraphic separation across the Jefferson fault similarly transitions northward from positive to negative (Figure 7). A klippe of Jefferson Formation truncates a fold in the Pilgrim Formation likely associated with reverse slip on an ENE-dipping splay of the SRF (Figure 4A).

Younger-on-older relationships across set (4) faults may be related to (A) impingement of out-of-sequence thrust faults into a pre-existing fold (i.e., fault-fold interaction), or (B) extensional reactivation of thrust faults. In interpretation (A), reverse faulting of the SRF between ~95 Ma and 75 Ma (Figure 2A) uplifted basement rock in its hanging-wall and generated an associated NNW-trending fault-propagation fold in overlying Paleozoic rocks. The Melrose fault, accomodating top-ENE slip, was impeded by this basement uplift, deformed internally—duplicating the Flathead Formation—and passed slip to set (4) faults higher in the section. Slipping out-of-sequence, set (4) faults then cut into this basement-cored fold, producing anomalous younger-on-older relationships where interaction was most pronounced (Figures 3A, 3B, and 7). Similar interaction between basement-cored folds and out-of-sequence thin-skinned thrust faults has been demonstrated in the Tendoy Mountains, ~80 km SSW of the study area (McDowell, 1997). In interpretation (B), set (3) and (4) faults comprise thrust faults reactivated as low-angle extensional detachments. Reactivation of the Melrose fault was likely underway by ~80 Ma, as indicated by thermochronologic model results (Figure 2A). Slightly later cooling of the Melrose fault hanging-wall may reflect extensional reactivation of faults higher in the section. However, extensional slip on at least the Lodgepole fault must have ceased by ~74 Ma, when it was cross-cut by a granodiorite (Figure 1B). Reactivation was apparently concentrated in the north, where superposed thick- and thin-skinned deformation contributed to greater graviational potential energy (Figures 3A, 3B, and 7). In this case, these faults would comprise the earliest and foreland-most examples of largely brittle synconvergent extension in the United States Cordillera and the first recognized instance in Montana, where possible examples of Cretaceous extension are confined to ductile, mid-crustal rocks further west (e.g., Lonn and others, 2003; Lonn and McDonald, 2004; Neal, 2022). Possibly analogous Late Cretaceous synconvergent extension localized to areas of basement uplift has been demonstrated in the Eureka culmination of Nevada (e.g., Long and others, 2015).

DESCRIPTION OF MAP UNITS

Qaf — Alluvial fan deposit (Holocene)—Gravel, sand, and silt deposited in small alluvial fans along range front and in Moose and Camp Creek drainages. Thickness as much as 10 m (Vuke, 2004).

Qc — Colluvium (Holocene and Pleistocene)—Pebble-gravel clasts with a sand, silt, and clay matrix. Deposited on slopes. Sparse boulder clasts are smaller than in QTdf. Thickness ≤ 6 m (Vuke, 2004).

Qac — Alluvium and colluvium (Holocene and Pleistocene)—Unconsolidated pebbles, sand, silt, and clay deposited on gentler slopes and Divide Valley floor. Thickness as much as 4.5 m (Vuke, 2004).

Qls — Landslide deposit (Holocene and/or Pleistocene)—Unconsolidated sediments and bedrock blocks transported by mass wasting events. Occurs dominantly on steep slopes in northern map area.

Qat — Alluvium of alluvial terrace (Holocene and Pleistocene)—Alluvium deposits adjacent to the Big Hole River. Generally covered by fine sediment and soil. Unknown thickness.

QTdf — Debris flow deposit (Pleistocene and Pliocene?)—Gravel deposits with subangular boulders as much as 1.5 m in diameter, dominantly of Belt Supergroup quartzite. Deposits are thicker (≤ 22 m) south of Soap Gulch than to the north (6 m; Vuke, 2004).

Tsc — Sixmile Creek Formation (Miocene and Pliocene?)—North of Soap Gulch, clasts are angular and dominantly of the LaHood Formation (informal Melrose unit of Vuke, 2004; undivided Paleogene sediments of O'Neill and others, 1996). South of Soap Gulch, occurs as isolated deposits of yellowish-red to brownish-gray angular to rounded pebbles, cobbles, and small boulders of mainly quartzite and minor granitic rock in sand matrix. Clasts of the Flathead Formation are common. May represent remnant of broad fluvial apron derived from the west (Neogene gravels of O'Neill and others, 1996).

Tca — Renova Formation, Climbing Arrow member (Eocene and Oligocene)—Dominantly red siltstone and shale, greenish-brown bentonitic mudstone, and yellowish micaceous clay/siltstone. Exposed thickness ~60 m (Vuke, 2004).

Edf — Debris flow deposit (Eocene)—Locally derived, matrix-supported, cobble to boulder clasts. Interlayered with Ev in the southern map area. Clasts are mainly angular to subrounded blocks up to 6 m in diameter of Proterozoic and Paleozoic sedimentary rock and Cretaceous granites.

Ev — Volcanic Rocks (Eocene)—Light browish-gray porphyritic basaltic andesite and andesite lava flows of up to 50 m in thickness. Yielded K-Ar ages of 47.7 ± 1.8 Ma to 51.8 ± 1.8 Ma (O'Neill and others, 1996). Likely equivalent to Lowland Creek Volcanics (~46–54 Ma; Olson and others, 2016).

TKdg — Diorite and gabbro (Late Cretaceous–Paleocene)—Small plugs of medium- to coarse-grained intermediate to mafic rock in the eastern portion of the map area.

TKl — Lamprophyre (Cretaceous–Tertiary)—Porphyritic sill-like lamprophyre intruding the Wolsey Formation. Up to ~200 m thick in the south map area and thins northward to < 1 m sill. A possibly corellative sill intrudes the Meagher Formation north of Camp Creek.

Kmg — Granodiorite and quartz monzonite of Moose Creek pluton (Late Cretaceous)—Medium- to coarse-grained dominantly porphyritic muscovite-biotite quartz monzonite containing phenocrysts of alkali feldspar and quartz. Dated at 74.2 ± 0.5 Ma via zircon U-Pb (du Bray and others, 2009).

Kg — Granite, granodiorite, and quartz monzonite, undivided (Late Cretaceous)—Fine- to medium-grained hyperabyssal intrusions dominantly within Mesoproterozoic sedimentary rocks in the northern map area. A small body intrudes Paleozoic sedimentary rocks in the western map area, cross-cutting a low-angle fault. This intrusion yielded a weighted mean zircon U-Pb age of 74.40 ± 0.37 | 0.72 Ma. While O'Neill and others (1996) interpretted this unit is contemporaneous with the Elkhorn Mountain Volcanics (~85–81 Ma; Olson and others, 2016), our age suggests later intrusion coeval with the Moose Creek pluton (see above).

Mmc — Mission Canyon Formation (Upper and Lower Mississippian)—Olive- to yellowish-gray, weathering to light-gray, medium- and thick-bedded to massive, very fine- to coarse-grained limestone. Locally includes bedded and nodular chert. Upper part of formation contains pale-red to grayish-orange limestone solution breccia (O'Neill and others, 1996). Thickness not well constrained in map area, but is ~300 m proximally west of the map area (O'Neill and others, 1996).

Mmlw — Lodgepole Formation, Woodhurst member (Lower Mississippian)—Medium- to dark-gray, fine- to medium-grained thick-bedded limestone grading upward to massive limestone. Contains abundant fragmented bioclastic material, especially at top of section. Thickness about 15 m.

Mmlp — Lodgepole Formation, Paine member (Lower Mississippian)—Medium- to dark-gray and brownsh-gray thin-bedded, laminated, and argillaceous limestone with thin beds and bed partings of dark-gray shale and shaley, mottled limestone (O'Neill and others, 1996). Thickness about 30 m.

MDts — Three Forks and Sappington formations, undivided (Mississippian and Devonian)—The Three Forks Formation consists of three members. The lowermost Logan Gulch member comprises yellowish-gray and grayish-red argillaceous limestone and evaporite breccia. The overlying Knoll Limestone is a petroliferous bioturbated mud limestone which varies in thickness (0–10 m), filling topography incised into the Logan Gulch member. The uppermost Trident Member consists of lower brownish-tan limestone beds, an interval of greenish-gray fissile shale, and upper fossiliferous gray limestone beds. The underlying Sappington Formation locally consists of black to gray shale and sandy siltstone with abundant reddish-orange-weathering chert. Total thickness is ~15–40 m.

Dj — Jefferson Formation (Upper and Middle Devonian)—Yellowish-brown to dark, purpleish gray, mottled, resistant, medium- to thick-bedded, coarsely crystalline dolomite. Has a characteristic fetic odor. Locally contains minor beds of shale and dissolution breccia. The uppermost Birdbear Member is light gray, microcrystalline dolomite. Thickness locally ~150–190 m (Theodosis, 1956).

D€mr — Maywood and Red Lion formations, undivided (Devonian and Cambrian)—The Maywood Formation consists of medium-gray or purplish, finely crystalline dolomite interbedded with tan siltstone. Thickness is ~30 m (Hansen, 1952). The underlying Red Lion Formation (also referred to as the Snowy Range Formation, e.g., O'Neill and others, 1996) consists of mottled and ribboned grayish-red dolomite overlain by yellowish-brown to gray dolomite. Contains intervals of laminated algal beds and domal to columnar stromatlites in upper part. Thickness is ~25 m (Hanson, 1952).

€pi — Pilgrim Formation (Middle and Upper Cambrian)—Medium- to light-gray mottled, thick- to massively-bedded, resistant, fine-grained dolomite, and thin-bedded, laminated, slope-forming dolomite. Mottling less conspicuous than in Meagher Formation. Upper part contains beds of fine- to medium-grained yellowish-tan sandstone. Thickness is ~60–100 m. Age from assignment to Cedaria–Aphelaspis faunal zones by Thomas (2007) and references therein.

€p — Park Formation (Middle Cambrian)—Green, finely micaceous, fissile shale with minor thin-bedded, yellowish-brown dolomite and yellowish-gray calcareous fine-grained sandstone, siltstone, and mudstone. Thickness in southern map area is ~40 m, thins to the north (O'Neill and others, 1996).

€m — Meagher Formation (Middle Cambrian)—Medium- to dark-gray and yellowish-brown fine- to medium-grained resistant limestone mottled with lighter gray, black, gold, or rust-colored irregular dolomite that grades into gray limestone or dolostone with closely spaced irregular tan or rust-colored dolomitic shale partings and oolitic or pelloidal limestone. Thickness near Camp Creek is ~180 m and thins to ~50 m to the north (Hanson, 1952; O'Neill and others, 1996).

€w — Wolsey Formation (Middle Cambrian)—Olive green, irregularly bedded, micaceous, fissile shale and fine-grained arkosic sandstone interbedded with olive-green, grayish-red, and reddish-brown siltstone and thin limestone. Metamorphosed to cordierite-bearing hornfels near contact with Moose Creek pluton in northern map area. Thickness along Camp Creek is 70 m (Hanson, 1952).

€f — Flathead Formation (Lower and/or Middle Cambrian?)—Very light gray, pinkish-gray, or yellowish-brown quartz arenite or orthoquartzite. Commonly contains a quartz pebble conglomerate at the base. Planar crossbeds and subordinate, grayish-green to pale-red, micaceous, fissile shale beds are common. Thickness as much as 20 m. Likely tectonically duplicated north of Camp Creek, where two quartzite units are observed. Tectonically juxtaposed against Paleoproterozoic basement south of the Camp Creek Fault and depositionally overlies Mesoproterozoic sedimentary rock north of this fault.

Yr — Ravalli Group (Mesoproterozoic)—Dominantly quartzite to siltite couples and couplets consisting of interbedded white to light-gray, fine- to medium-grained, quartz arenite to orthoquartzite from 1 cm to 0.5 m thick, containing distinctive well-rounded, frosted quartz grains, alternating with thinner reddish-orange siltstone beds that are < 10 cm thick. Some couplets are normally graded and planar cross-bedding is present in some quartzite beds. Mapped as Missoula Group by O'Neill and others (1996). Maximum thickness in map area is < 100 m, but unit thickness eastward to ~ 200 m. Unit is absent in the northeastern map area, where the Flathead Formation overlies the Greyson Formation.

Ygc — Greyson Formation, upper calcsilicate member (Mesoproterozoic)—Dominantly planar greenish-gray quartzite, siltite, and argillite. Interbedded in microcouplets and couplets containing calc-silicate minerals (McDonald and others, 2012). Soft-sediment deformation, small-scall flaser bedding, and mudcracks are common. Thickness in map area is < 100 m; unit thickens to east to ~140 m in central Highland Mountains (O'Neill and others, 1996; McDonald and others, 2012). Mapped as Spokane Formation by O'Neill and others (1996).

Yg, Ygq — Greyson Formation, lower argillite member—Dominantly drab-olive, very thin and planar beds of siltstone and argillite. Uncommon, 0.2 to > 2 m-thick, lenticular beds of tan to white thin ripple-cross-laminated beds of very fine-grained quartzite and thinly laminated intervals of very planar dark gray argillite/claystone are present (designated Ygq, where mappable). Uniformly underlies the Greyson Formation, upper calcsilicate member, but interfingers with the underlying LaHood Formation, dark argillite facies. Unit is ~200 m thick in map area but thickens to >1 km in central Highland Mountains (O'Neill and others, 1996; McDonald and others, 2012).

Ylad, Yladc — LaHood Formation, dark argillite and carbonate facies—Dark gray to pinkish-gray argillite and silty argillite. Beds are 1–3 cm, massive, and interbedded with tan siltstone with flat laminae or very fine-grained quartzite. Beds are tabular and have very planar parting surfaces (O'Neill and others, 1996). Laterally discontinuous zones of dolomitic to calcareous dolomite, commonly associated with finely crstalline medium-gray limestone, are present (designated Yladc, where mappable). Carbonaceous intervals reach thicknesses of > 150 m, as measured in the M-20 borehole. Sulfide mineralization—dominantly disseminated and bedded chalcopyrite and pyrite—is present throughout this facies but is most intense in calcareous to dolomitic intervals. Mapped as Newland Formation by O'Neill and others (1996). Interfingers with overlying Greyson Formation throughout the map area and likely interfingers with the underlying LaHood Formation argillite and siltite facies north of Old Glory Mountain. Absent in the eastern map area. Unit is thickest to the northeast of northwest-striking fault splays of the North and South Rochester faults. Maximum thickness exceeds 275 m.

Ylaa — LaHood Formation, argillite and siltite facies (Mesoproterozoic)—Medium-gray to tan argillite and siltite with minor white to light-gray quartzite. Lacks diagnostic tabular, blocky beds of overlying dark argillite facies and the arkosic sand grains of the underlying intermediate siliciclastic facies. Partially interfingers with the underlying intermediate siliciclastic facies and the overlying dark argillite and carbonate facies. Mapped as Moose Formation by O'Neill and others (1996). Thickness ranges from < 40 m in the western map area to ~80 m in the eastern map area. Unit exhibits facies and thickness changes across northwest-striking faults (O'Neill and others, 1996).

Ylai — LaHood Formation intermediate siliciclastic facies (Mesoproterozoic)—Interbedded argillite, siltite, and subordinate channels of gravel conglomerate and poorly sorted argillaceous arkosic sandstone. Lacks clean quartzite of overlying facies and cobble conglomerate of underlying facies. Interfingers with underlying and overlying facies. Estimated thickness ≤ 1 km in map area. Roughly equivalent to LaHood Formation distal facies of O'Neill and others (1996).

Ylac — LaHood Formation, conglomeratic facies (Mesoproterozoic)—Cobble to boulder conglomerate near the Camp Creek Fault. Grades laterally into pebble conglomerate then into coarse argillaceous, lithic and arkosic sandstone. Generally structureless and massively bedded, although normally graded sequences with planar laminations occur in eastern map area near North Rochester Fault. Interfingers with overlying intermediate siliciclastic facies. Thickest proximally north of the Camp Creek Fault, but thick tongues are present within intermediate facies, especially adjacent to fault splays. The SG-1 borehole, which did not reach basement, intersected ~320 m of conglomerate below the Camp Creek Fault, comprising a minimum thickness of this facies.

Xag — Amphibolite gneiss (Paleoproterozoic?)—Dark-gray to black, fine-grained equigranular intrusions, metamorphosed to amphibolite. Contain hornblende, plagioclase, augite, and garnet. Exist as pods and dikes within Xbgg and Xmbg.

Xog — Orthogneiss (Paleoproterozoic)—Granitic to granodioritic foliated orthogneiss. Present as large (~5 km²) sill-like body in and near Camp Creek. Associated with granite, aplite, and pegmatite sills and dikes. Dated at 1,797.7 ± 16.5 Ma via zircon U-Pb geochronology (Carrapa and others, 2019).

Xlg — Leucocratic gneiss (Paleoproterozoic?)—Muscovite-rich lenses and pods of leucocratic gneiss within Paleoproterozoic orthogneiss.

Xmbg — Mylonitic biotite gneiss (Paleoproterozoic)—Dark-gray to black, medium- to coarse-grained, sillimanite-bearing, biotite-rich gneiss. Contains strongly folded foliation and porphyroblasts of quartz and plagioclast which are sheared or augen.

Xbgg — Biotite-garnet gneiss (Paleoproterozoic)—Dark-gray to black, medium- to very coarse-grained, strongly folded, garnet-rich biotite gneiss with abundant thin ptygmatic quartz-feldspar veins. Zircon U-Pb geochronology yielded a maximum depositional age for the sedimentary protolith of this unit of 1,794.2 ± 3.0 Ma, with little evidence for post-depositional metamorphic growth of zircon (Figure 1A). Designated Archean by McDonald and others (2012) and Early Proterozoic and Archean by O'Neill and others (1996).

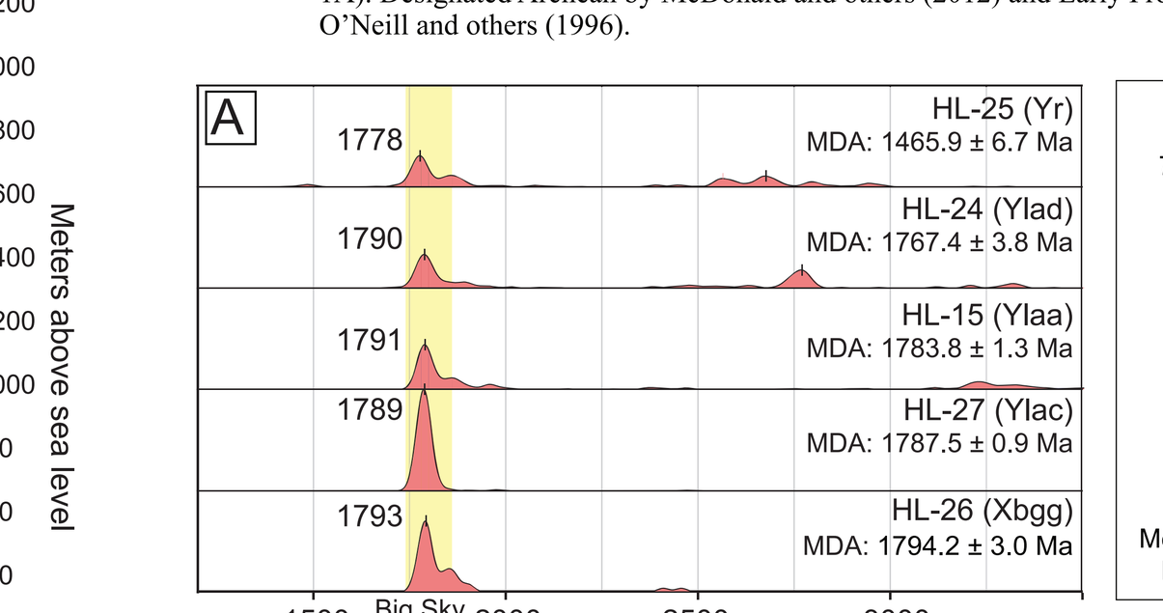

Figure 1: (A) Stacked kernel density estimate plots (kernel bandwidth = 15 Myr) showing results of zircon U-Pb analyses from the Highland Mountains. A sample of the volumetrically dominant basement lithology, biotite-garnet gneiss (Xbgg), yielded entirely Paleoproterozoic ages (HL-26). Samples from Mesoproterozoic Belt Supergroup yielded probability peaks similar to this basement sample, suggesting local provenance. Maximum depositional ages (MDAs) are indicated, calculated as the weighted average of the youngest cluster of ages overlapping at 2σ uncertainty. (B) The weighted mean age of a granodioritic pluton cross-cutting the Lodgepole fault constrains slip to prior to ~74 Ma.

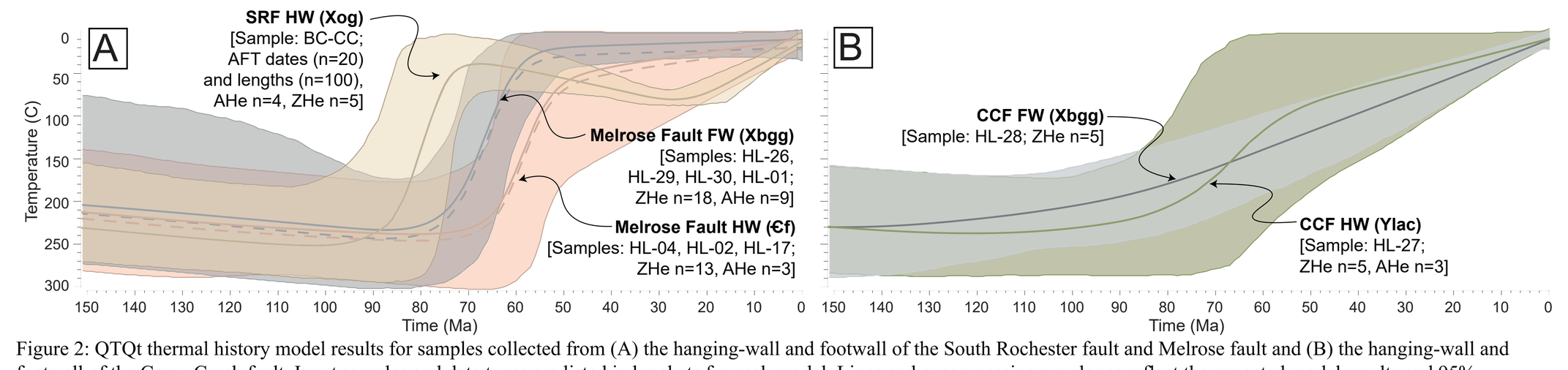

Figure 2: QTQt thermal history model results for samples collected from (A) the hanging-wall and footwall of the South Rochester fault and Melrose fault and (B) the hanging-wall and footwall of the Camp Creek fault. Input samples and data types are listed in brackets for each model. Lines and encompassing envelopes reflect the expected model results and 95% credible intervals. In QTQt, the expected model is a weighted mean model where the weighing is provided by the posterior probability. Where samples were modeled as a vertical profile, dashed line reflects expected model result for the lowest sample in the profile, while solid line reflects that for the highest sample in the profile. Abbreviations: AFT—apatite fission track; AHe—apatite (U-Th-Sm)/He; CCF—Camp Creek fault; HW—hanging-wall; FW—footwall; SRF—South Rochester fault; ZHe—zircon (U-Th)/He.

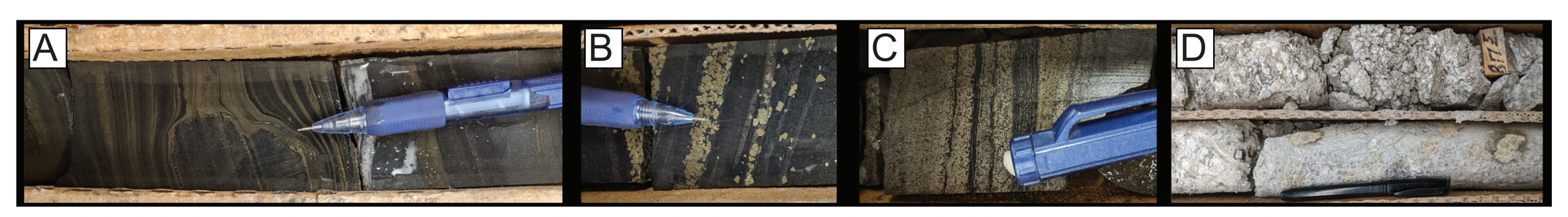

Figure 3: (A–C) Drill core from the M-20 borehole showing stratiform pyrite and chalcopyrite mineralization in the dark argillite and carbonate facies of the LaHood Formation. Key features include: (A) soft sediment deformation (at 347 m); (B) euhedral mm-to-cm pyrite (at 395 m); (C) intense mineralization along bedding planes (at 389 m). (D) Fault gouge and breccia observed at ~250 m depth in drill core from borehole SG-1.

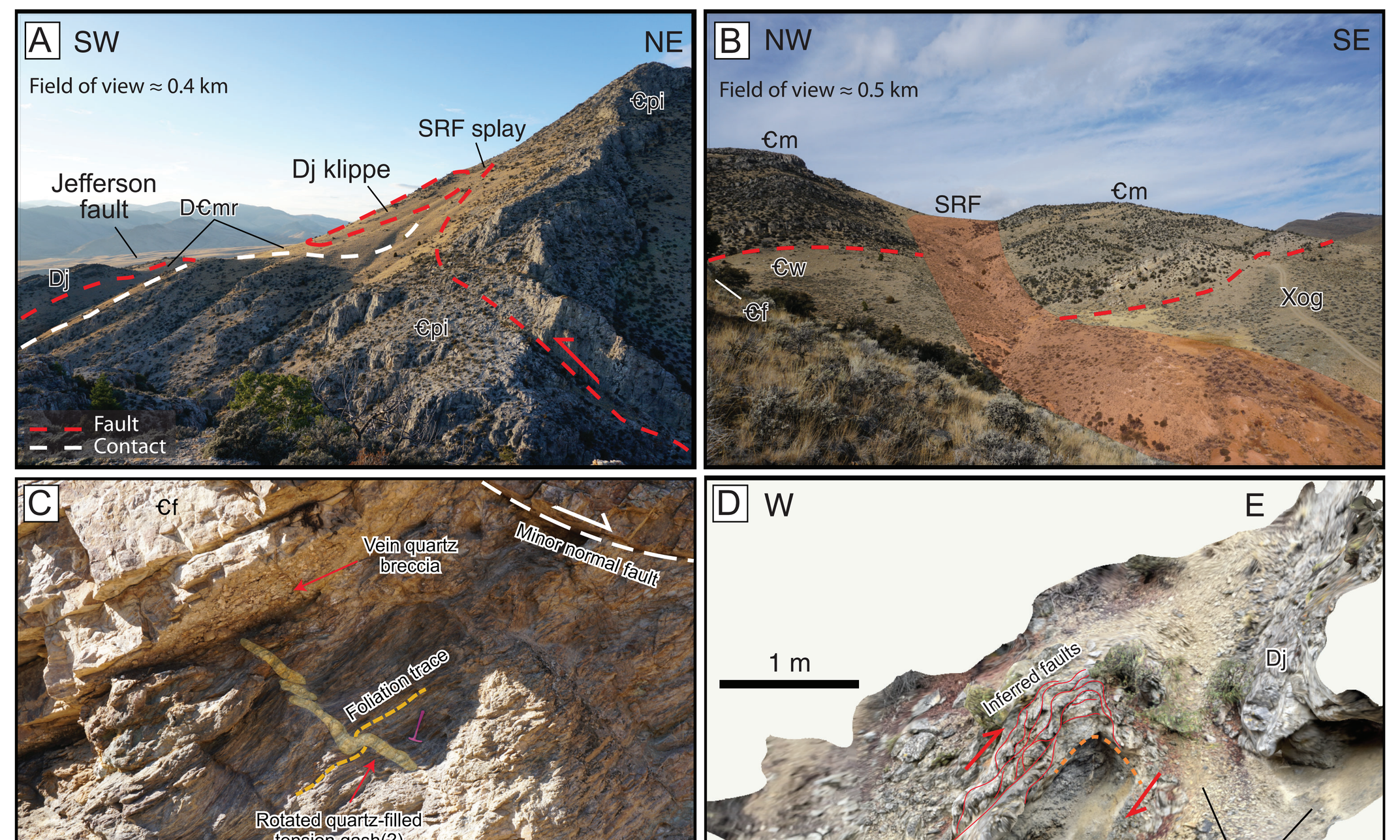

Figure 4: (A) Looking northwest toward the klippe of Jefferson Formation in the west-central map area, which truncates folded Cambrian units. The Pilgrim Formation is thrust over itself in the middleground by a steep reverse fault linked to the South Rochester Fault (SRF). (B) Looking northeast across the SRF from Camp Creek. The Meagher Formation is juxtaposed against Precambrian basement northeast of the SRF, omitting the Wolsey and Flathead formations. Down-dropping of the Meagher Formation associated with normal reactivation of the SRF is evident. (C) The Melrose fault north of Camp Creek is marked by brecciated vein quartz. Foliation within the sheared chlorite schist has been folded around a rotated quartz-filled tension gash (highlighted in yellow) in an S-shaped manner. This may comprise a vein-related antithetic slip-reverse drag fold, indicative of top-WSW shear (e.g., Druguet, 2019). The outcrop is cut by N-dipping normal faults with m-scale slip. Rock hammer is highlighted in pink. (D) LIDAR scan of the Lodgepole fault zone north of Camp Creek, where a klippe of Mississippian Lodgepole Formation is in fault contact with Devonian Jefferson Formation. The fault surface dips 41° toward an azimuth of 227°. Asymmetrically folded cleavage planes (dashed orange line) define a fold hinge pluning 18° toward an azimuth of 145° (i.e., out-of-page). Imbricated horses within the upright limb of the fold are outlined in red.

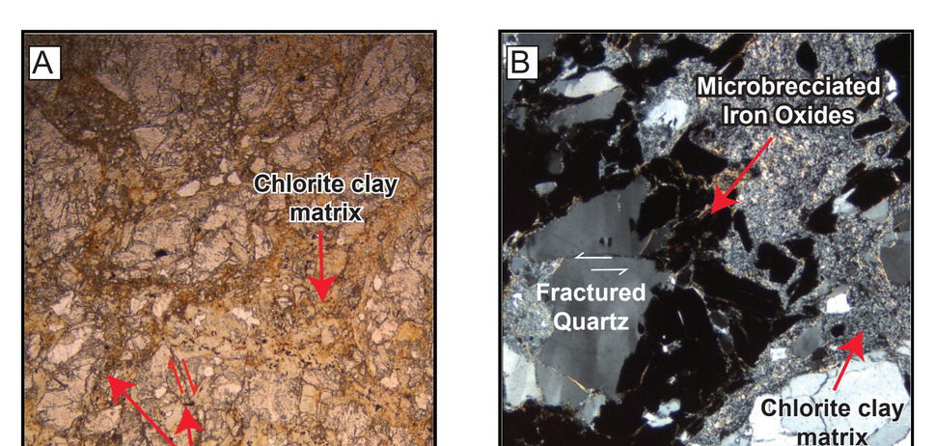

Figure 5: (A) Plane-polarized photomicrograph of sample HL-14 from the South Rochester Fault shear zone near Soap Gulch, showing microbrecciation of quartz and plagioclase feldspar with seritic alteration and chlorite clay matrix (~40 % by volume), consistent with brittle deformation. (B) Cross-polarized photomicrograph of sample HL-34 from the Melrose fault zone, showing fracturing of quartz, microbreciation of iron oxides, and chlorite clay matrix (~30 % by volume), consistent with brittle deformation at the Cambrian–Paleoproterozoic contact.

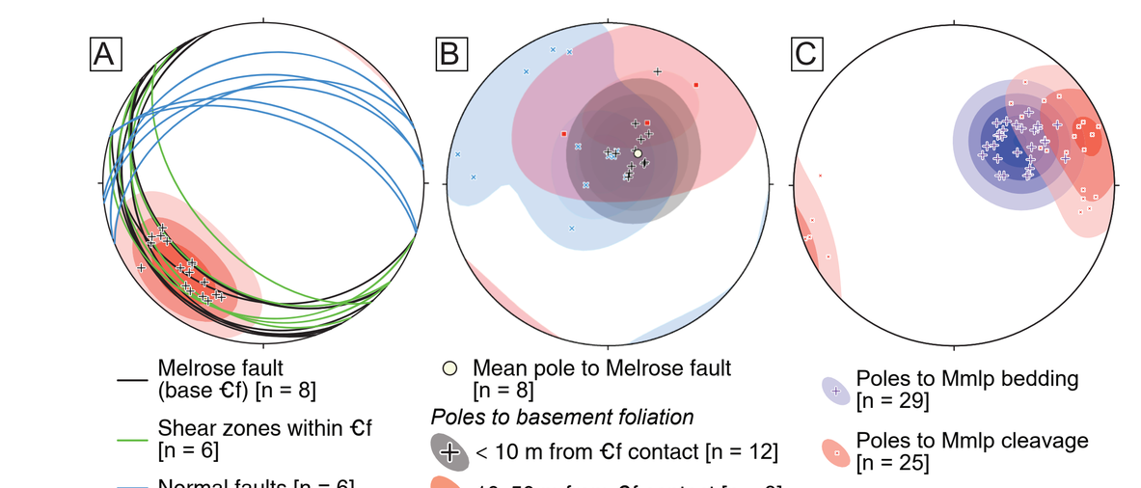

Figure 6: (A) Structural data from the Melrose fault zone: fault zone boundary, shear zones within the Flathead Formation, minor normal faults, and slickenlines on the fault zone boundary (base of the Flathead Formation). (B) Poles to metamorphic foliation in Proterozoic basement are widely spread > 50 m from the Melrose fault but systematically rotate to become subparallel to the fault zone boundary within ~10 m of the contact. (C) Pressure solution cleavage in the Mississippian Lodgepole Formation is near-vertical, while bedding dips moderately to the southwest.

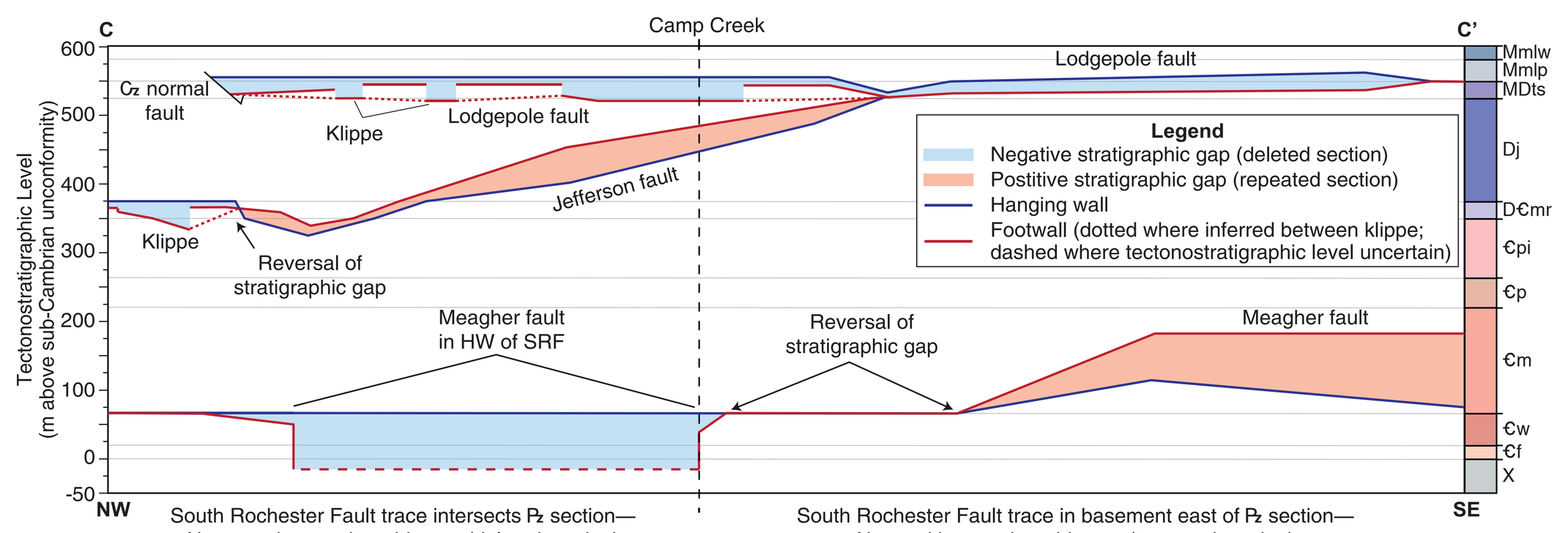

Figure 7: Stratigraphic separation diagram showing several key faults in the southeastern study area. Faults were projected into the plane of the C–C′ line shown on the main map (only end segments of line shown for clarity). Portions of faults across which section is deleted are shown in blue (i.e., younger-on-older), while portions across which section is repeated are shown in red (i.e., older-on-younger). Minor faults and splays are not shown. The Melrose fault is not shown due to uncertain position of footwall. Net fault displacement decreases from southeast to northwest, with a significant transition from net repetition to net deletion of section occuring near Camp Creek, where the South Rochester Fault trace intersects the Paleozoic section.

REFERENCES

Andretta, D.B., 1961, Geology of the Moose Creek stock, Highland Mountains, Montana [PhD Thesis]: Montana State University, Bozeman, Montana.
Brandon, W.C., 1984, An origin for the McCartney's Mountain salient of the southwestern Montana fold and thrust belt [Master of Science]: University of Montana, Missoula, Montana.
du Bray, E., Lund, K., and Tilling, R.I., 2009, Geochemical database for the Boulder batholith and its satellite plutons, southwest Montana: USGS, southwest Montana data series.
Brumbaugh, D.S., 1973, Structural Analysis of the complexly deformed Big Hole River area, Beaverhead, Madison, and Silver Bow counties, Montana [Ph.D. Dissertation]: Indiana University, Bloomington, Indiana.
Carrapa, B., DeCelles, P.G., and Romero, M., 2019, Early Inception of the Laramide Orogeny in Southwestern Montana and Northern Wyoming: Implications for Models of Flat-Slab Subduction: Journal of Geophysical Research: Solid Earth, v. 124, p. 2102–2123, doi:10.1029/2018JB016888.
Condit, C.B., Mahan, K.H., Ault, A.K., and Flowers, R.M., 2015, Foreland-directed propagation of high-grade tectonism in the deep roots of a Paleoproterozoic \ collisional orogen, SW Montana, USA: Lithosphere, doi:10.1130/L460.1.
DeCelles, P.G., 2004, Late Jurassic to Eocene evolution of the Cordilleran thrust belt and foreland basin system, western U.S.A.: American Journal of Science, v. 304.
Druguet, E., 2019, Deciphering the presence of axial-planar veins in tectonites: Geoscience Frontiers, v. 10, p. 2101–2115, doi:10.1016/j.gsf.2019.02.005.
Elliott, C.G., and McDonald, C., 2009, Geologic map and geohazard assessment of Silver Bow County, Montana: Montana Bureau of Mines and Geology Open-File Report 585, 88p., 3 sheets, scale 1:50,000.
Fox, N.R., 2017, Sedimentary tectonics of the Mesoproterozoic LaHood Formation, southwest Montana: [M.Sc. Thesis]: Montana State University, Bozeman, Montana.
Gallagher, K., 2012, Transdimensional inverse thermal history modeling for quantitative thermochronology: Transdimensional inverse thermal history: Journal of Geophysical Research: Solid Earth, v. 117, no. B2.
Hanson, A.M., 1952, Cambrian Stratigraphy in Southwestern Montana: Montana Bureau of Mines and Geology Memoir 33.
Kulik, D.M., and Schmidt, C.J., 1988, Region of overlap and styles of interaction of Cordilleran thrust belt and Rocky Mountain foreland, in Schmidt, C.J. and Perry, W.J., Jr. eds., Interaction of the Rocky Mountain Foreland and the Cordilleran Thrust Belt: Geological Society of America.
Lageson, D.R., 1989, Reactivation of a Proterozoic continental margin, Bridger Range, southwestern Montana: Montana Geologic Society, 1989 Field Conference Guidebook: Montana Centennial Edition, v. 1, p. 279–298.
Long, S.P., Thomson, S.N., Reiners, P.W., and Di Fiori, R.V., 2015, Synorogenic extension localized by upper-crustal thickening: An example from the Late Cretaceous Nevadaplano: Geology, v. 43, p. 351–354.
Lonn, J.D., and McDonald, C., 2004, Geologic map of the Kelly Lake 7.5′ quadrangle, southwestern Montana: Montana Bureau of Mines and Geology, 1 sheet, 1:24:000 scale.
Lonn, J.D., McDonald, C., Lewis, R.S., Kalakay, T.J., O'Neill, J.M., Berg, R.B., and Hargrave, P., 2003, Preliminary geologic map of the Philipsburg 30′x60′ quadrangle, western Montana: Montana Bureau of Mines and Geology, 1 sheet, 1:100,000 scale.
McDonald, C., Elliot, C., Vuke, S., Lonn, J., and Berg, R., 2012, Geologic Map of the Butte South 30′ X 60′ quadrangle, southwestern Montana: Montana Bureau of Mines and Geology, 1 sheet, 1:100,000 scale.
McDowell, R.J., 1997, Evidence for synchronous thin-skinned and basement deformation in the Cordilleran fold-thrust belt: the Tendoy Mountains, southwestern Montana: Journal of Structural Geology, v. 19, p. 77–87.
McMannis, W.J., 1963, LaHood Formation—A Coarse Facies of the Belt Series in Southwestern Montana: GSA Bulletin, v. 74, p. 407–436.
Neal, B.A., 2022, The Montana Alps: Kilometer-scale recumbent folding and tectonic attenuation in the Anaconda Range, Southwestern Montana [M.Sc. Thesis]: Montana State University, Bozeman, Montana.
Nilsen, T.H., 1991, Stratigraphy and depositional systems of the Precambrian Belt Supergroup in theWhitehall Area, southwestern Montana, Report 91THN-9, submitted to Golden Sunlight Mines, Inc.
Olson, N.H., Sepp, M.D., Dilles, J.H., Mankins, N.E., Blessing, J.M., and Scarberry, K.C., 2017, Geologic map of the Mount Thompson 7.5′ quad- rangle, southwest Montana: Montana Bureau of Mines and Geology EDMAP-11, scale 1:24,000.
O'Neill, J.M., 1995, Table Mountain Quartzite and Moose Formation (new names) and associated rocks of the middle Proterozoic Belt Supergroup, Highland Mountains, southwestern Montana: U.S. Geologic Survey Bulletin 2121A.
O'Neill, J.M., Ferris, D.C., Schmidt, C.J., and Hanneman, D.L., 1986, Recurrent movement along northwest-trending faults at the southern margin of the Belt Basin, Highland Mountains, southwestern Montana: Belt Supergroup: Montana Bureau of Mines and Geology Special Publication, v. 94, p. 209–216.
O'Neill, J.M., Klepper, M.R., Smedes, H.W., Hanneman, D.L., Fraser, G.D., and Mehnert, H.H., 1996, Geologic map and cross sections of the central and southern Highland Mountains, southwestern Montana: U.S. Geologic Survey Miscellaneous Field Studies Map I-2525.
O'Neill, J.M., Schmidt, C.J., and Genovese, P.W., 1990, Dillon cutoff-Basement-involved tectonic link between the disturbed belt of west-central Montana and the overthrust belt of extreme southwestern Montana: Geology, v. 18, p. 1107–1110.
Richards, R.W., and Pardee, J.T., 1925, The Melrose phosphate field, Montana: U.S. Geological Survey Bulletin 780-A, 32 p., 2 plates, scale 1:62,500.
Ruppel, E.T., and Lopez, D.A., 1984, The thrust belt in Southwest Montana and east-central Idaho: U.S.Geologic Survey Professional Paper 1278, 45 p.
Ruppel, E.T., O'Neill, J., and Lopez, D.A., 1983, Preliminary geologic map of the Dillon 1° x 2° Quadrangle, Montana: U.S. Geological Survey Open-File Report 83–163, scale 1:250,000.
Schmidt, C. J., & Garihan, J. M. (1983). Laramide tectonic development of the Rocky Mountain foreland of southwestern Montana. In J. D. Lowell (Ed.), Rocky Mountain foreland basins and uplifts (pp. 271–294): Rocky Mountain Association of Geologists.
Smedes, H.W., Klepper, M.R., and Tilling, R.I., 1988, Preliminary map of plutonic units of the Boulder batholith, southwestern Montana: U.S. Geological Survey Open-File Report 88–283.
Theodosis, S.D., 1956, The geology of the Melrose area, Beaverhead and Silver Bow counties, Montana [Ph.D. Dissertation]: Indiana University, Bloomington, Indiana.
Thomas, R., 2007, A field guide to the Cambrian section at Camp Creek, southwest Montana: Northwest Geology, v. 36, p. 231–244.
Vuke, S.M., 2004, Geologic map of the Divide area, southwest Montana: Montana Bureau of Mines and Geology Open-File Report 502, 36p., 1 sheet, scale 1:50,000.
White, J., Gammons, C.H., and Zieg, G., 2014, Paragenesis of cobalt and nickel in the Black Butte shale-hosted copper deposit, Belt Basin, Montana, USA: Mineralium Deposita, v. 49, p. 335–351.
Winston, D., 1986, Sedimentation and Tectonics of the Middle Proterozoic Belt Basin and Their Influence on Phanerozoic Compression and Extension in Western Montana and Northern Idaho: Part II. Northern Rocky Mountains: v. 155, p. 87–118.
Zieg, G.A., 1981, Stratigraphy sedimentology and diagenesis of the Precambrian upper Newland Limestone central Montana [M.Sc. Thesis]: University of Montana, Missoula, Montana.

MBMG
Montana Bureau of Mines and Geology
EDMAP 16

Geologic Map of the Eastern Half of the Melrose 7.5′ Quadrangle and the Western Half of the Wickiup Creek 7.5′ Quadrangle, Southwestern Montana

Chance B. Ronemus and Devon A. Orme
Montana State University-Bozeman

2023